


Article

A Novel Control Method of Clutch During Mode Transition of Single-Shaft Parallel Hybrid Electric Vehicles

Jingang Ding^{1,2} and Xiaohong Jiao^{1,*} 

¹ School of Electrical Engineering, Yanshan University, Qinhuangdao 066004, China; dingjingang@126.com

² Power Center, Baic Motors CO.LTD Automotive Research Institute, Beijing 101106, China

* Correspondence: jiaoxh@ysu.edu.cn

Received: 23 November 2019; Accepted: 27 December 2019; Published: 30 December 2019



Abstract: The mode transition of single-shaft parallel hybrid electric vehicles (HEVs) between engine and motor has an important impact on power and drivability. Especially, in the process of mode transition from the pure motor-drive operating mode to the only engine-drive operating mode, the motor starting engine and the clutch control problem have an important influence on driving quality, and solutions have a bit of room for improving dynamic performance. In this paper, a novel mode transition control method is proposed to guarantee a fast and smooth mode transition process in this regard. First, an adaptive sliding mode control (A-SMC) strategy is presented to obtain the desired torque trajectory of the clutch transmission. Second, a proportional-integral (PI) observer is designed to estimate the actual transmission torque of the clutch. Meanwhile, a fractional order proportional-integral-differential (FOPID) controller with the optimized control parameters by particle swarm optimization (PSO) is employed to realize the accurate position tracking of the direct current (DC) motor clutch so as to ensure clutch transmission torque tracking. Finally, the effectiveness and adaptability to system parameter perturbation of the proposed control approach are verified by comparison with the traditional control strategy in a MATLAB environment. The simulation results show that the driving quality of the closed-loop system using the proposed control approach is obviously improved due to fast and smooth mode transition process and better adaptability.

Keywords: hybrid electric vehicles (HEVs); mode transition; adaptive sliding mode control (A-SMC); clutch actuator; PI observer; fractional order proportional-integral-differential (FOPID)

1. Introduction

Hybrid electric vehicles (HEVs) have received extensive attention from the automotive industry and academia, and are widely regarded as one of the most effective solutions to the growing use of petroleum fuels for transportation and environmental problems [1,2]. HEVs possessing multiple power sources have different working modes, the control strategy for the vehicle determines the working mode according to the driver's intention and the driving state of the car [3]. The hybrid system equipped with an automatic clutch and an electric motor (EM) has to perform the mode transition process from the pure electric driving mode to the engine-on driving mode in most conditions, in which the engine needs to be started and engaged into the driveline via the clutch [4–6]. In this process, the differences in response characteristics of each power source and the change of the state of the transmission or the clutch may cause a sudden change in engine or motor torque, which may lead to a non-negligible impact on the powertrain system [7,8]. Therefore, control approaches with high performance need to be developed to guarantee the fast and smooth process of mode transition.

During the mode transition of the single-shaft hybrid powertrain, the engine can be started and engaged into the driveline by the clutch. The performance of mode transition mainly relies on the

quality of the clutch control [9,10], hence, the control of clutch engagement remains an important and challenging issue during mode transition. Some researchers have dedicated much valuable work to achieve fast and smooth clutch engagement control of mode transition for HEVs. For example, a nonlinear feedforward-feedback controller and PID algorithm are developed in [10] to effectively improve both riding comfort and engine-start time of a P2 hybrid vehicle. A robust control-based hierarchical mode transition control approach is proposed in [11] to reduce the mode transition time and obtain acceptable vehicle jerk. The double closed-loop control strategy is designed in [12] to control the clutch transmitting required torque of engine-start process, which contains a fuzzy method as an outer loop and a modified predictive functional method as an inner loop. Although the dynamic process and the control objectives of the clutch engagement process of mode transition of the single-shaft parallel hybrid powertrain are significantly different from that of the conventional vehicle, the dry clutch engagement control design of the conventional vehicle could be a reference to the clutch control of mode transition process. For the clutch control of the conventional vehicle, many effective approaches have been put forward. A model predictive control approach is developed in [13] to comply with constraints to ensure a comfortable lockup and to avoid the stall of the engine as well as to reduce the clutch engagement time. For example, a model predictive control method with the correction of clutch wear is proposed in [14] based on the estimation of resistance torque to achieve precise position control of the clutch. A modified predictive functional control approach with a sliding mode observer is proposed in [15] to obtain a satisfying performance for the automated clutch control of vehicle. The optimal control method is designed in [16] to generate the reference trajectories of the clutch slip speed and motor torque to provide satisfactory performance even under large variation of vehicle mass and road grade. Moreover, another approach has been extensively studied and utilized, such as triple-step control method [17,18] and backstepping control method [19] are adopted to solve the optimal trajectory tracking problem to achieve accurate clutch control.

Motivated by the aforementioned analysis, in this paper, aiming at further improving the control performance of clutch engagement during the mode transition from the pure motor-drive operating mode to the only engine-drive operating mode, a novel control method is proposed to solve the vehicle jerk and clutch slipping energy loss issues of mode transition process. The main feature of the proposed method has three aspects. One is that adaptive sliding mode control (A-SMC) is introduced into the clutch transmission torque command to generate the desired clutch transmission torque trajectory based on the rotating speed difference between the clutch driving and driven discs. The second is that the unmeasurable actual transmission torque of the clutch is estimated by a PI observer employing the EM speed. The third is that the realization of the clutch transmission torque tracking is accomplished through a fractional order proportional-integral-differential (FOPID) controller with the optimized control parameters by particle swarm optimization (PSO), which results in performing the accurate position tracking of the direct current (DC) motor clutch.

The rest of the paper is organized as follows. In Section 2, the dynamic models of the driveline of a single-shaft parallel powertrain and the automatic dry clutch actuating mechanism are built. In Section 3, the mode transition control strategy is designed. Simulation results and discussions are given in Section 4. Finally, the paper is concluded in Section 5.

2. System Modeling

In this paper, a single-shaft parallel powertrain with the automated mechanical transmission (AMT) is investigated, as shown in Figure 1. It consists of a conventional engine, automatic dry clutch, electric motor (EM), and a five-speed AMT. The clutch is controlled to perform the mode transition. In this system, the clutch is placed inside the drive motor. This HEV can operate in a variety of driving modes: pure electric driving mode, pure engine driving mode, hybrid driving mode, engine active charging mode, and regenerative braking mode. When the vehicle speed reaches the switching threshold, the hybrid control unit (HCU) will send the mode transition signal to the transmission control unit (TCU). When the TCU receives the mode transition signal, the clutch will quickly start

to engage. Furthermore, the HCU will send the torque command to the EM control unit (MCU) and the engine control unit (ECU) to satisfy the driving torque of the vehicle. The main parameters of the single-shaft parallel vehicle are given in Table 1.

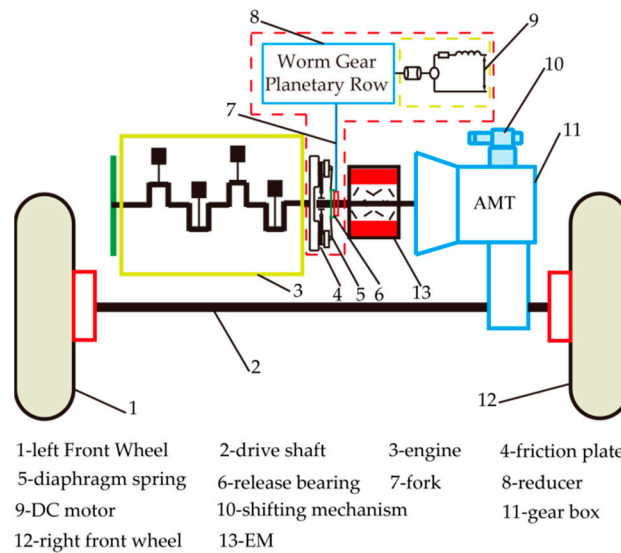


Figure 1. Structure of single-shaft parallel hybrid powertrain.

Table 1. Main parameters of single-shaft parallel hybrid vehicle.

Components	Description
Engine	Max torque: 150 Nm, peak power: 78 kW.
Electric motor (EM)	Permanent magnet synchronous motor (PMSM), max torque: 80 Nm, peak power: 30 kW.
Clutch	Max torque: 180 Nm.
Automated mechanical transmission (AMT)	Gear ratios: 3.583, 1.956, 1.327, 0.968, 0.702. Final gear ratio: 4.05.
Battery	Lithium iron phosphate battery, capacity: 10 Ah, nominal voltage: 288 V.

2.1. Powertrain System Dynamic Modeling

The models of main components of the single-shaft parallel hybrid powertrain related to the mode transition process are given in this part. Based on the configuration characteristics of the single-shaft parallel hybrid powertrain, the simplified schematic of the powertrain model in a mode transition process is presented for the design of the control strategy in Figure 2. Where T_e , T_c , T_m and T_r are the engine torque, the clutch torque, the EM torque and the vehicle resistant torque, respectively. ω_e and ω_m represent the engine speed and the EM speed, respectively. I_e , I_m and I_r represent the engine inertia moment, the EM inertia moment and the vehicle inertia moment, respectively. i_a and i_g are the gear ratio and the final gear ratio of AMT, respectively.

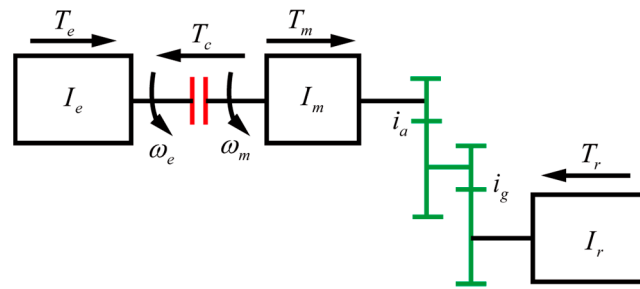


Figure 2. Simplified model sketch of mode transition.

Assuming that the tires slip is ignored, and according to the vehicle longitudinal dynamics, the vehicle resistant torque can be calculated as follows [20]:

$$T_r = (mgf \cos \alpha + \frac{C_D A v^2}{21.15} + mg \sin \alpha) r_w \quad (1)$$

where m , g , f , α , C_D , A , v and r_w are vehicle mass, gravity acceleration, rolling resistance coefficient, road slope angle, air resistance coefficient, frontal area of the vehicle, vehicle speed, and wheel radius, respectively.

In this paper, according to the clutch operating characteristics [12], the mode transition process from EM driving mode to engine driving mode is divided into three stages:

(i) Clutch disengaged stage

During this stage, the engine is still, the clutch is in the disengaged state, and the vehicle is solely driven by the EM. The dynamical equation of this stage can be expressed as follows:

$$T_m = T_v + (I_v + I_m) \dot{\omega}_m \quad (2)$$

where $I_v = I_r / (i_a^2 i_g^2)$ is the equivalent inertia moment of the vehicle at the EM output shaft. $T_v = T_r / (i_a i_g)$ is the equivalent load torque of hybrid powertrain on the EM output shaft.

(ii) Clutch slipping stage

In this stage, the clutch starts to engage after receiving the command from the TCU, and the EM is used to start the engine and drive the vehicle simultaneously. The dynamical equation during this stage can be expressed as follows:

$$T_m = T_v + T_c + (I_v + I_m) \dot{\omega}_m \quad (3)$$

$$T_c = I_e \dot{\omega}_e - T_e \quad (4)$$

$$\begin{cases} T_e = -b_e \omega_e, & \omega_e \leq \omega_{fire} \\ T_e = f(\beta, \omega_e), & \omega_e > \omega_{fire} \end{cases} \quad (5)$$

where b_e , ω_{fire} and β are engine frictional coefficient, engine idle speed and engine throttle opening angle, respectively. $f(\beta, \omega_e)$ represents that the engine torque is a nonlinear function of the engine speed and the throttle opening angle.

The clutch torque can be expressed as follows [21]:

$$T_c = \mu_k r_c n F_n \text{sign}(\omega_m - \omega_e) \quad (6)$$

where μ_k is the frictional coefficient, r_c is the effective radius of the clutch disk, n is the number of clutch plate, F_n is the pressing force on the plates. $sign(\cdot)$ is the sign function described as follows:

$$sign(\omega_m - \omega_e) = \begin{cases} 1, & \omega_m - \omega_e > 0 \\ 0, & \omega_m - \omega_e = 0 \\ -1, & \omega_m - \omega_e < 0 \end{cases} \quad (7)$$

At this stage, the engagement speed of the clutch has an important influence on the quality of the mode transition. In order to meet the longitudinal jerk of the vehicle, the engagement time should be minimized to avoid unnecessary energy loss of slipping friction.

(iii) Clutch engaged stage

In this stage, the clutch is engaged fast, the vehicle is driven by both engine torque and EM torque. The dynamic equation can be described as follows:

$$T_e + T_m = T_v + (I_e + I_m + I_v)\dot{\omega}_m \quad (8)$$

2.2. Clutch System Dynamic Modeling

The schematic diagram of the automatic dry clutch system is shown in the red dotted frame of Figure 1. As shown in Figure 1, the clutch system consists of dry clutch and actuating mechanism. The actuating mechanism includes a direct current (DC) motor used as impetus, worm gear and planetary row employed as transmission mechanism to reduce speed. The rotational motion of the motor is transformed into linear motion via the transmission mechanism, and the release bearing can be released by the release fork.

According to Newton's second law and Kirchhoff's law, the DC motor's voltage balance equation and torque balance equation [17] can be described as follows:

$$L_d \dot{i}_d = u_d - R_d i_d - K_b \omega_d \quad (9)$$

$$I_d \dot{\omega}_d = K_a i_d - K_c \omega_d - T_{CL} \quad (10)$$

where L_d , ω_d , I_d , i_d , R_d and u_d are the armature inductance, the motor rotational angle velocity, the motor rotational inertia moment, the armature current, the armature resistance and the battery voltage, respectively. K_a , K_b and K_c are the torque constant, the Back electromotive force (EMF) constant and the frictional coefficient, respectively. T_{CL} is the load torque of the motor.

Assuming that the actuating mechanism has no mechanical deformation, and according to mechanical transmission principle, the dynamics of the actuating mechanism is described as follows:

$$T_{CL} = I_{eq} \dot{\omega}_d + \frac{F_{xth} L}{\eta_t i_t} \quad (11)$$

$$\theta_d = \frac{y_c}{L} i_t \quad (12)$$

where I_{eq} is the equivalent inertia moment at the DC motor output shaft. L , i_t and η_t is the release fork arm length, the transmission ratio and the transmission efficiency of the actuating mechanism, respectively. θ_d is the motor rotational angle. F_{xth} is the return force of diaphragm spring. y_c is the release bearing position. Moreover, it is difficult to build an accurate model to calculate the return force of diaphragm spring, so the test data from the clutch manufacturer is used in this paper to regard as a lookup table in simulation, the relationship between F_{xth} and y_c is shown in Figure 3.

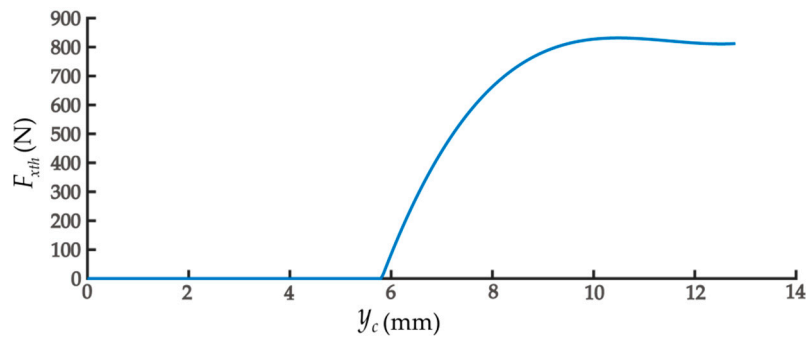


Figure 3. Relationship between spring pressure and release bearing position.

3. Mode Transition Controller Design

According to the stage division described in Section 2.1, the flow chart of the mode transition process from EM driving mode to engine driving mode is shown in Figure 4.

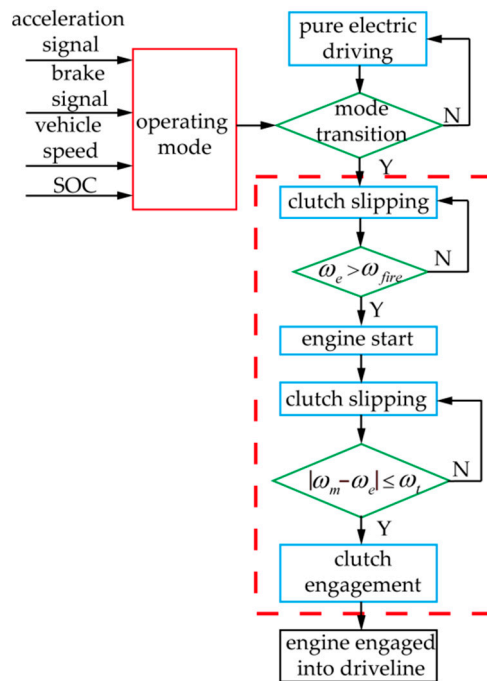


Figure 4. Flow chart of the mode transition from EM driving to engine driving.

Firstly, the clutch disengaged begins to engage. Due to the driven disk not touching the active disk, the clutch doesn't transmit torque and the engine speed is zero. Secondly, as the clutch position continuously increases, the driven disk of clutch moves past the free displacement, the clutch begins to slip and transmit torque to the engine for speed increase. When the engine speed reaches and exceeds the idle speed, the engine begins to fire and then will be synchronized with EM via the ECU. Finally, the clutch engages rapidly and the engine is engaged into the powertrain. However, the fixed clutch engagement speed will cause excessive slipping energy loss and vehicle jerk. Therefore, the mode transition control problem could be converted to clutch control problem to achieve the fast and smooth mode transition. The vehicle jerk and the slipping energy loss are crucial indexes of mode transition performance, which can be described as follows:

$$\begin{cases} j = \frac{da}{dt} \\ w = \int_{t1}^{t2} T_c |\omega_m - \omega_e| dt \end{cases} \quad (13)$$

where j is the vehicle jerk. w is the slipping energy loss. t_1 and t_2 are the starting time and stopping time of the clutch sliding process, respectively. a is the vehicle acceleration.

The effect of clutch control is characterized by the following requirement:

- (1) The vehicle jerk is controlled within 10 m/s^3 during the clutch engagement process;
- (2) The mode transition time should be within 1 s;
- (3) The engine doesn't turn off during the mode transition process;
- (4) The clutch slipping energy loss should be as little as possible during the mode transition process.

The schematic diagram of the proposed control approach to mode transition from EM driving mode to engine driving mode is shown in Figure 5.

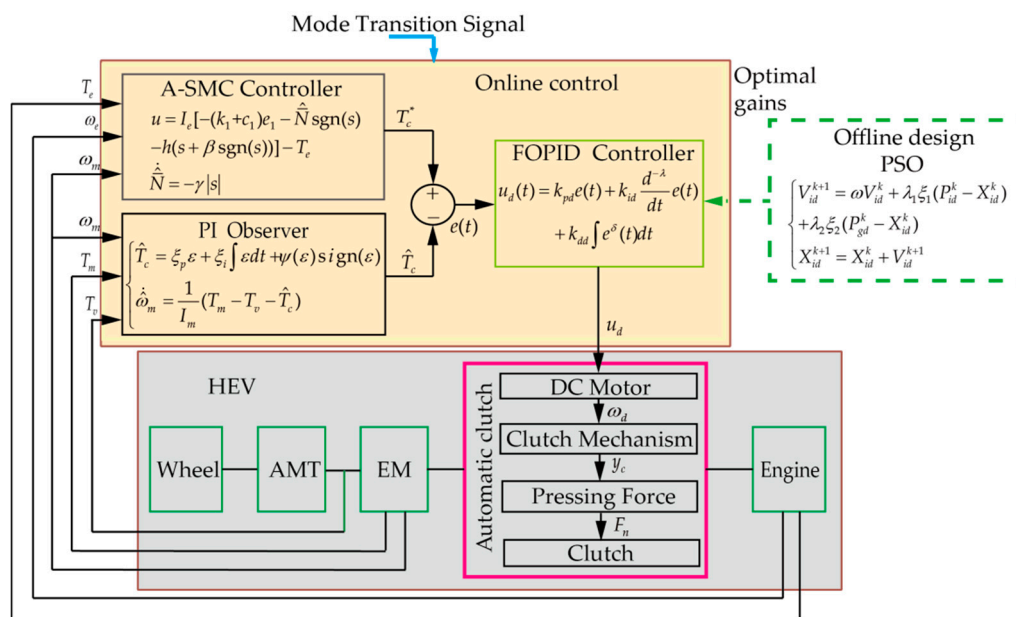


Figure 5. Schematic diagram of the proposed control method.

From Figure 5, it can be seen that the proposed control strategy consists of two parts: the design of clutch torque command and the torque tracking control. In the consideration of the nonlinear dynamics of the clutch engagement and some uncertainties existing in this process, the A-SMC technique is adopted to generate the clutch torque command. Moreover, considering that the transmitted torque of the dry clutch is usually not measurable, a PI observer is designed to estimate the actual clutch torque. Meanwhile, a FOPID controller is adopted to control the torque tracking. Because FOPID is recognized to guarantee better performance besides the simplicity realization and fine stability of the classical PID controller due to the more flexibility and more robust in presence of parameters' uncertainties both in the controlled system and the controller itself [22,23]. Similar to classical PID, the controller parameters of FOPID should be defined in advance by the designer. To overcome time-consuming of the manual tuning and fractional calculus, an optimal tuning method is required to determine the control parameters of FOPID. In this paper, PSO is adopted to optimize the control parameters of FOPID offline.

3.1. Design of Clutch Torque Command based on A-SMC

Engine and EM should be considered together to design the clutch torque command. In light of nonlinear dynamics of the clutch engagement and uncertainty during the mode transition process, an A-SMC-based generator of the clutch torque command is designed.

According to the powertrain dynamic Equations (3) and (4), the state variables and the control variable of the powertrain system are selected as:

$$x = \omega_e, x_d = \omega_m, e_1 = x - x_d, e_{1\alpha} = \int (x - x_d) dt, u = T_c^*$$

the system model can be expressed as follows:

$$\begin{cases} \dot{e}_{1\alpha} = e_1 \\ \dot{e}_1 = \frac{1}{I_e}(u + T_e) + N \end{cases} \quad (14)$$

where N represents the whole disturbance resulting from the clutch engagement process including the effect from the EM, which is not measurable but bounded with $|N| \leq \bar{N}$, \bar{N} is regarded as an unknown constant although it can be estimated by the limit value of the worst case, which can be handled by adaptive technique instead of robust control.

Therefore, the control law $u = T_c^*$ will be designed based on the sliding mode control and the adaptive backstepping technique. Furthermore, there is the following proposition.

Proposition 1. For the powertrain system (3)–(4) operating the mode transition from the motor driving to engine driving, the reference trajectory of the clutch torque during the clutch engagement process can be generated by the output of an adaptive sliding mode controller designed as follows:

$$T_c^* = u = I_e[-(k_1 + c_1)e_1 - \hat{N}\text{sgn}(s) - h(s + \beta\text{sgn}(s))] - T_e \quad (15)$$

with adaptive update law:

$$\dot{\hat{N}} = -\gamma|s| \quad (16)$$

and a sliding mode surface:

$$s = k_1 e_{1\alpha} + e_2 \quad (17)$$

where $e_2 = e_1 + c_1 e_{1\alpha}$. \hat{N} is the estimate of the unknown constant \bar{N} . c_1, k_1, h, β and γ are adjustable positive real values, and c_1, k_1, h should be chosen satisfying the following condition:

$$c_1 + hk_1^2 > 0, h(c_1 + k_1) > \frac{1}{4} \quad (18)$$

Proof. Firstly, a Lyapunov function is constructed as follows:

$$V_1 = \frac{1}{2}e_{1\alpha}^2 \quad (19)$$

considering e_2 as the virtual control, the time derivative of V_1 is calculated as:

$$\dot{V}_1 = e_{1\alpha}\dot{e}_{1\alpha} = e_{1\alpha}e_2 - c_1e_{1\alpha}^2 \quad (20)$$

And then, a Lyapunov function for the system (14) is constructed as follows:

$$V_2 = V_1 + \frac{1}{2}s^2 \quad (21)$$

considering (20), it follows:

$$\dot{V}_2 = e_{1\alpha}e_2 - c_1e_{1\alpha}^2 + s\left[k_1e_1 + \frac{1}{I_e}(u + T_e) + N - \dot{x}_d + c_1e_1\right] \quad (22)$$

Therefore, when the control law u is designed as (15) with (17), the following inequality holds.

$$\dot{V}_2 \leq e_{1\alpha}e_2 - c_1e_{1\alpha}^2 - hs^2 - h\beta|s| + \bar{N}|s| - \hat{N}|s| = -e^T Qe - h\beta|s| + \bar{N}|s| \tag{23}$$

where

$$Q = \begin{bmatrix} c_1 + hk_1^2 & hk_1 - \frac{1}{2} \\ hk_1 - \frac{1}{2} & h \end{bmatrix}, e^T = [e_{1\alpha}, e_2], \bar{N} = \bar{N} - \hat{N}$$

Finally, a Lyapunov function for the whole closed-loop system is constructed as follows:

$$V_3 = V_2 + \frac{1}{2\gamma}\bar{N}^2 \tag{24}$$

considering (23), the time derivative of V_3 satisfies the following inequality.

$$\dot{V}_3 \leq -e^T Qe - h\beta|s| + \bar{N}|s| - \frac{1}{\gamma}\bar{N}\dot{\bar{N}} \tag{25}$$

then, considering the adaptive update law (16), it follows:

$$\dot{V}_3 \leq -e^T Qe - h\beta|s| \tag{26}$$

Due to the condition (18), Q is a positive definite matrix so that $\dot{V}_3 \leq 0, \forall e, s, \bar{N}$, thus, the whole system is Lyapunov stable at the equilibrium ($e_{1\alpha} = 0, s = 0, \bar{N} = 0$). Furthermore, based on the principle of LaSalle’s invariant set, it follows that $e_1 \rightarrow 0$, namely, $\omega_e \rightarrow \omega_m$ as $t \rightarrow \infty$.

It means that if the clutch torque output is rendered as the trajectory T_c^* (15), the whole driveline dynamics during the clutch engagement process under the mode transition from motor driving to engine driving is stable and the engine speed can be synchronized with motor speed. Meanwhile, it should be noted from (26) that the convergence rate of $\omega_e \rightarrow \omega_m$ is dependent on Q, β , namely, is closely related to the choice of the adjustable parameters c_1, h, k_1, β . Thus, for better convergence performance, these parameters should not be too small, but they should not be too large to avoid oscillations in the trajectory under the premise of satisfying the condition (18). □

3.2. Design of PI Observer

The dry clutch system has a strong nonlinearity and many factors have an effect on the clutch engagement performance, such as the plate temperature and the slipping speed. Therefore, it is difficult to accurately calculate and measure the transmitted torque of the dry clutch in engineering. For this regard, according to [24,25], a PI observer is designed to estimate the transmitted torque of the dry clutch.

The actual transmitted torque of the dry clutch can be expressed as follows:

$$\begin{cases} T_c = T_{c0} + \Delta(\varepsilon) \\ |\Delta(\varepsilon)| \leq \psi(\varepsilon) \\ \varepsilon = \hat{\omega}_m - \omega_m \end{cases} \tag{27}$$

where T_{c0} is the initial transmitted torque, $\psi(\varepsilon)$ is the bound of the unknown function $\Delta(\varepsilon)$, and $\hat{\omega}_m$ is the estimate of the EM speed. Thus, a PI observer of the transmitted torque is designed as follows:

$$\begin{cases} \hat{T}_c = \xi_p \varepsilon + \xi_i \int \varepsilon dt + \psi(\varepsilon) \text{sign}(\varepsilon) \\ \dot{\hat{\omega}}_m = \frac{1}{I_m}(T_m - T_v - \hat{T}_c) \end{cases} \tag{28}$$

where ξ_p and ξ_i are the proportional gain and the integral gain of the PI observer, respectively.

The selection of the two parameters follows the principle that they should not be too small for the better convergence accuracy of the observer, but they should not be too large to avoid overshoot, that is to say, the compromise is required between better transient and steady-state performance. The detail can refer to the adjusting rules of PI gains presented in [25].

3.3. Design of Clutch Torque Tracking Controller

For guaranteeing the clutch transmission torque fast tracking the desired torque trajectory obtained by the SMC-based adaptive controller (21), a FOPID controller in the following form [26] is adopted to generate the voltage u_d of the DC motor to actuate the clutch.

$$u_d(t) = k_{pd}e(t) + k_{id}\frac{d^{-\lambda}}{dt}e(t) + k_{dd}\int e^\delta(t)dt \tag{29}$$

where $e(t) = T_c^*(t) - \hat{T}_c(t)$. k_{pd} , k_{id} and k_{dd} are the proportional, integral and differential gains, respectively, and λ and δ are positive coefficients of the fractional-order. The detail on the adjusting rules of FOPID parameters can refer to the description in [27], and to avoid the fractional calculus, an optimal tuning method is usually required to determine the control parameters of FOPID.

In this paper, the PSO algorithm is adopted to seek optimal gains of FOPID controller [28]. It should be noted that the PSO algorithm is executed offline to obtain the optimal parameters of FOPID. The schematic diagram of the parameter optimization offline and the flowchart of the PSO algorithm are shown in Figure 6.

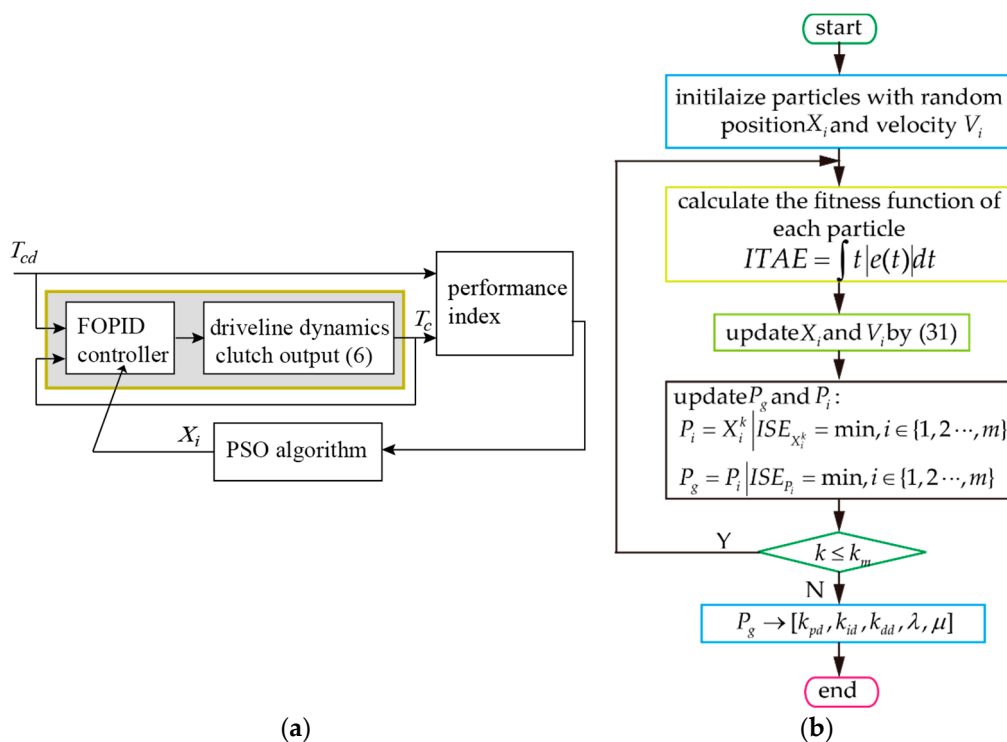


Figure 6. Schematic diagram of the particle swarm optimization (PSO) algorithm. (a) Schematic diagram of the parameter optimization offline, (b) flowchart of PSO.

In the algorithm, m is chosen as the number of particles, and each particle $X_i = [k_{pd}, k_{id}, k_{dd}, \lambda, \mu]$. The integrated time absolute error (ITAE) criterion is utilized as the fitness function, which can be described as follows:

$$ITAE = \int t|e(t)|dt \tag{30}$$

where $e(t) = T_{cd}(t) - T_c(t)$, $T_{cd}(t)$ is given as the idea trajectory of the clutch torque during the clutch engaging process, and $T_c(t)$ is the clutch torque output of the model (6) with the driveline dynamics established in Simulink. The update principles of the velocity V_i and position X_i of each particle during the iterations can be described as follows:

$$\begin{cases} V_{id}^{k+1} = \omega V_{id}^k + \lambda_1 \xi_1 (P_{id}^k - X_{id}^k) + \lambda_2 \xi_2 (P_{gd}^k - X_{id}^k) \\ X_{id}^{k+1} = X_{id}^k + V_{id}^{k+1} \end{cases} \quad (31)$$

where $i = 1, 2, \dots, m$, $d = 1, 2, \dots, 5$. k is iteration steps, $k = 0, 1, 2, 3, \dots, k_m$. P_i, P_g are the individual optimal position and global optimal position, respectively. λ_1 and λ_2 are acceleration factors that are non-negative constants. ξ_1 and ξ_2 are random numbers between 0 and 1.

In this paper, considering the calculation accuracy and the large computing burden of PSO, choose $m = 20$, $k_m = 100$, select $X_{imax} = [1,1,1,2,2]$ and $X_{imin} = [0.00001,0.00001,0.00001,0.00001,0.00001]$. The parameters are offline optimized as: $k_{pd} = 0.5$, $k_{id} = 0.5$, $k_{dd} = 0.0001$, $\lambda = 0.97$, $\delta = 0.83$.

4. Simulation Results

In this section, the simulation model of single-shaft parallel hybrid powertrain is built based on MATLAB/Simulink. It is worth mentioning that the system modelling presented in Section 2 is a control-oriented model, but the model with high fidelity in the simulation is further detailed in order to simulate the real vehicle powertrain more realistically, such as more realistic nonlinearity and complexity are modeled for the dynamical description of the whole driveline system, and the delays of the control transmission and measurement are also taken into account. The simulations of launching and accelerating process are carried out to verify the effectiveness of the proposed method. The driver’s demand torque in simulation is shown in Figure 7. The main system parameters of the studied hybrid powertrain are given in Table 2.

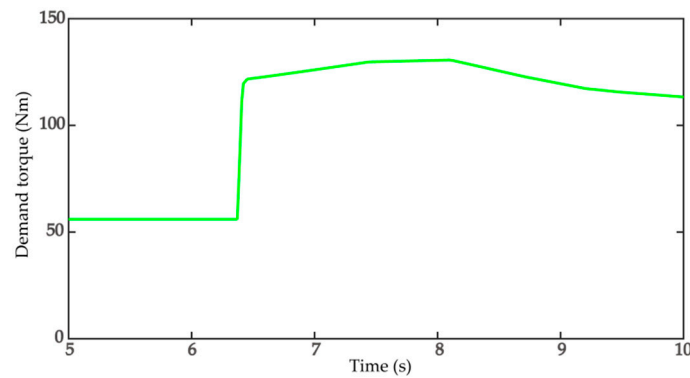


Figure 7. Driver’s demand torque.

Table 2. Main parameters of the simulation model.

Parameter	Value	Parameter	Value
m	1250 kg	ω_{fire}	800 r/min
g	9.8 m/s ²	L_d	0.0003 H
f	0.022	I_d	0.0001 kg m ²
α	0	R_d	0.2 Ω
C_D	0.9	K_a	0.041 V/(rad/s)
A	2.4 m ²	K_b	0.041 Nm/A
r_w	0.293 m	K_c	0.001 Nm/(rad/s)
I_e	0.2 kg m ²	J_e	0.003 kg m ²
I_m	0.1 kg m ²	L	0.045 m
I_r	1.9 kg m ²	i_t	135.8
b_e	0.025 Nm/(rad/s)	η_t	0.61

Moreover, in the simulation, according to the selecting principle presented as in the previous section, the control parameters of the A-SMC, PI observer and FOPID controller are chosen as:

$$c_1 = 0.8, k_1 = 0.3, h = 0.9, \beta = 2.5, \gamma = 0.1, \xi_p = 0.005, \xi_i = 1.1, \quad (32)$$

$$k_{pd} = 0.5, k_{id} = 0.5, k_{dd} = 0.0001, \lambda = 0.97, \delta = 0.83$$

4.1. Comparative Analysis

To evaluate the control performance of the proposed method, the comparison with the conventional engineering control method is presented. Firstly, Figure 8 shows the effect of the observer of the clutch torque.

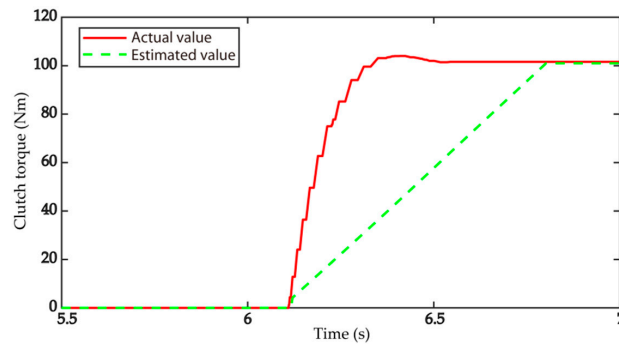


Figure 8. Result of PI observer.

As seen in the Figure 8, the estimated value of clutch torque converges to the actual value quickly in approximate 0.7 s, and the estimate error is within an acceptable scale.

Further, the comparison result during the mode transition from EM driving mode to engine driving mode is shown in Figure 9. Meanwhile, for clarifying the comparison on the control performance index, these comparison results are summarized in Table 3.

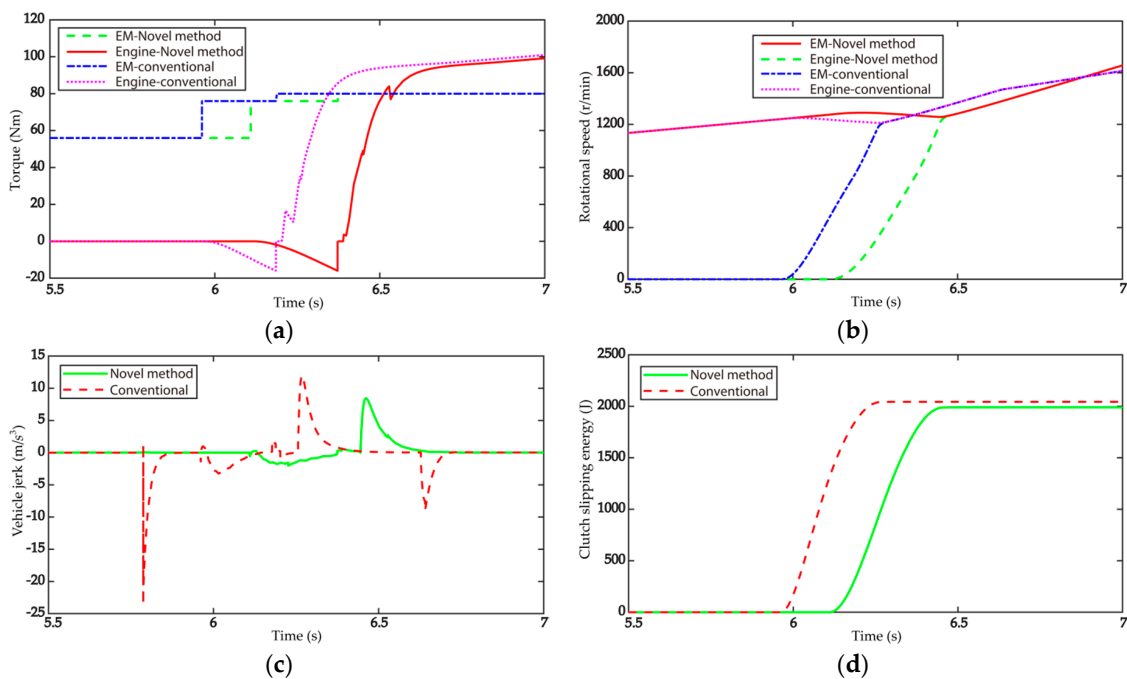


Figure 9. Comparison result in simulation. (a) Engine and EM torque, (b) engine and EM speed, (c) vehicle jerk, (d) clutch slipping energy loss.

Table 3. Summary of comparison results for two methods.

Performance Index	Proposed Novel Control	Conventional Control
Mode transition time [s]	0.75	0.6
Vehicle jerk [m/s^2]	8.1	23.9
Clutch slipping energy loss [J]	1976	2051

As shown in Figure 9a,b, and Table 3, the mode transition time of the proposed control method is 0.75 s, longer than that 0.6s of the conventional engineering control method, which is helpful to reduce the vehicle jerk. The whole mode transition process takes no more than 0.8 s and vehicle keeps accelerating in the novel method, which meets the control target. It can be seen from Figure 9c and Table 3, the maximum value of vehicle jerk 8.1 m/s^3 is less than 10 m/s^3 in the novel method during the mode transition process, which is far less than that 23.9 m/s^3 of conventional method. Moreover, the novel method generates less slipping energy loss 1976 J than that of conventional method 2015 J, shown in Figure 9d and Table 3. Comparison of vehicle jerk and slipping energy loss indicates the fast and smooth advantages of the novel control method.

4.2. Adaptability Analysis

Some system parameters may change as the system and road conditions change during the actual mode transition process of single-shaft parallel hybrid electric vehicles, such as the frictional coefficient b_e , vehicle mass m , rolling resistance coefficient f_r , road slope angle α , clutch mechanical deformation and so on. In this subsection, the vehicle jerk and clutch slipping energy loss of mode transition with different b_e , m and f_r are studied to verify the adaptability of the proposed novel control method. The simulation result is shown in Figure 10 and summarized in Table 4.

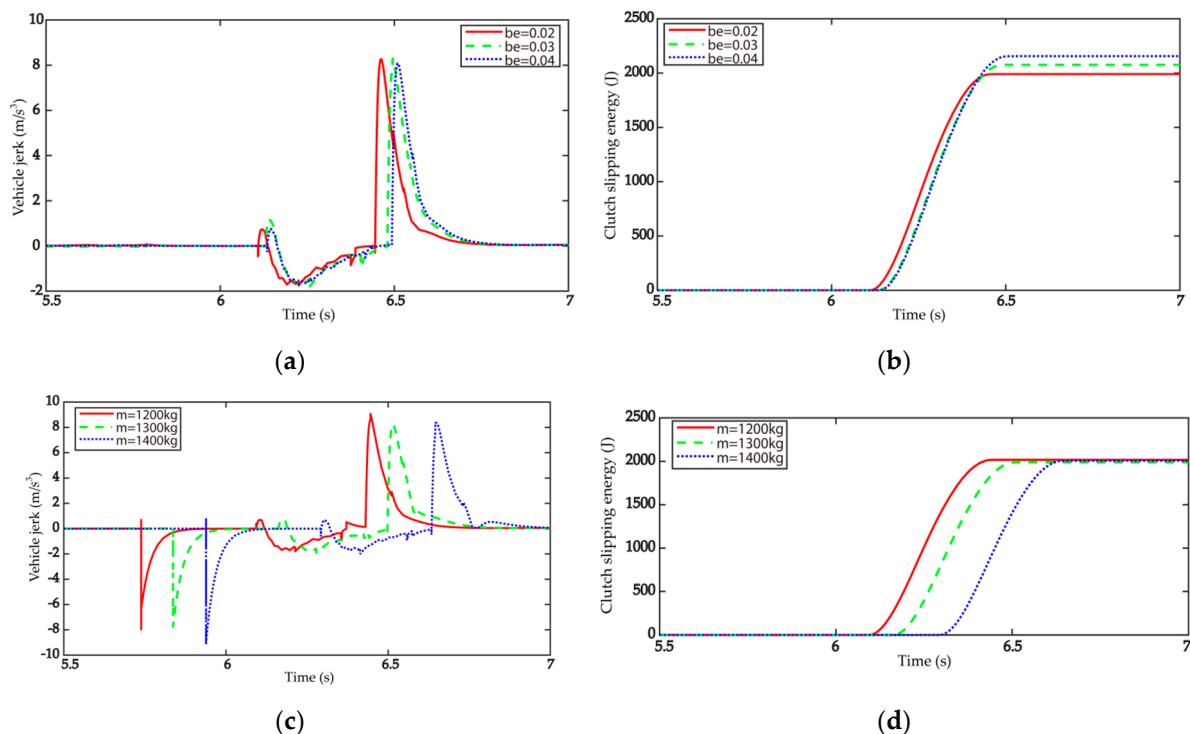


Figure 10. Cont.

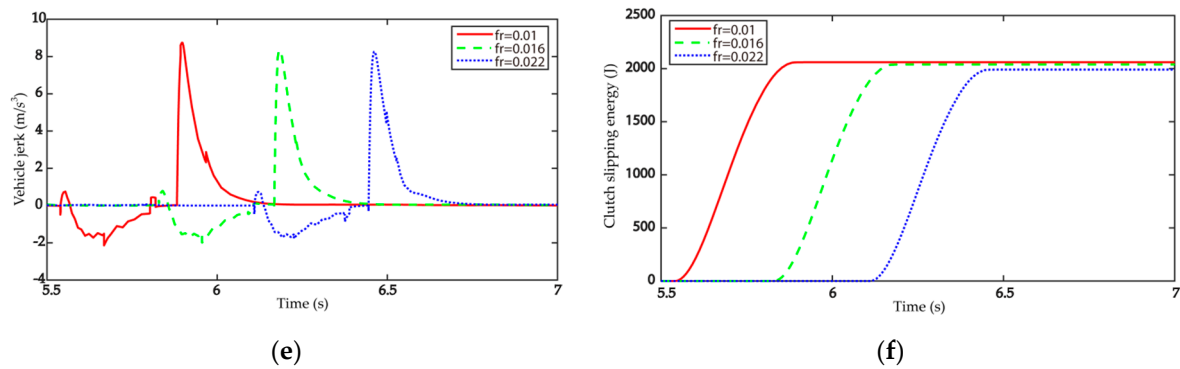


Figure 10. Comparison result for adaptability analysis. (a) Vehicle jerk under different engine frictional coefficients, (b) clutch slipping energy loss under different engine frictional coefficients, (c) vehicle jerk under different vehicle mass, (d) clutch slipping energy loss under different vehicle mass, (e) vehicle jerk under different rolling resistance coefficient, (f) clutch slipping energy loss under different rolling resistance coefficient.

Table 4. Summary of comparison results for different parameter variations.

Physical Name	Parameter Variation	Vehicle Jerk	Clutch Slipping Energy Loss
Frictional coefficient	$b_e = 0.02$	8.34	1990
	$b_e = 0.03$	8.31	2071
	$b_e = 0.04$	8.08	2152
Vehicle mass	$m = 1200$	9.01	2013
	$m = 1300$	8.21	1998
	$m = 1400$	8.45	2003
Rolling resistance coefficient	$f_r = 0.01$	8.95	2046
	$f_r = 0.016$	8.26	2031
	$f_r = 0.022$	8.23	1997

From Table 4, Figure 10a,b, it can be seen that both vehicle jerk and clutch slipping energy loss are very small in the different engine frictional coefficients 0.02, 0.03, 0.04. It indicates that the proposed novel control method is adaptive to different engine frictional coefficients. Similarly, as seen from Table 4, Figure 10c,d, and Figure 10e,f, the vehicle jerk and the clutch slipping energy loss are all very small in different vehicle masses 1200 kg, 1300 kg, 1400 kg, and different rolling resistance coefficients 0.01, 0.015, 0.022. These demonstrate that the proposed novel control method is adaptive to different vehicle masses and rolling resistance coefficients.

5. Conclusions

A novel control strategy of mode transition from EM driving to engine driving has been developed to reduce vehicle jerk and slipping friction energy loss for a single-shaft parallel hybrid powertrain in this paper. The proposed control strategy includes a SMC-based adaptive controller obtaining the desired clutch torque, a FOPID controller actuating the clutch mechanism to track the desired clutch torque, and a PI observer estimating the unmeasurable actual clutch torque. These three parts cooperate well to accomplish the mode transition from the EM driving mode to the engine driving mode with satisfactory control performance. For better tracking control performance, a PSO algorithm is used to optimize the control parameters of the FOPID offline. Both theoretical analysis and the simulation comparison with the traditional control strategy verify this point. Moreover, the simulation results under various physical parameter variations also show that the proposed novel control method is adaptive to system parameter perturbation.

In this paper, the effects of the clutch wear isn't taken into account in the controller design, so mode transition control considering more performance index including clutch wear will be studied in future work.

Author Contributions: J.D. wrote the original draft, designed the control method, drew the figures and performed the simulations. X.J. was responsible for supervising this research and involved in exchanging ideas, reviewing and revising the article draft. All authors have read and agreed to the published version of the manuscript.

Funding: This research was funded by the National Natural Science Foundation of China (Grant No. 61573304 and No. 61973265) and the Natural Science Foundation of Hebei Province (Grant No. F2017203210).

Conflicts of Interest: The authors declare no conflict of interest.

References

1. Fu, X.; Ma, J.; Zhang, Q.; Wang, C.; Tang, J. Torque Coordination Control of Hybrid Electric Vehicles Based on Hybrid Dynamical System Theory. *Electronics* **2019**, *8*, 712. [[CrossRef](#)]
2. Zhou, Y.; Ravey, A.; Péra, M. A Survey on Driving Prediction Techniques for Predictive Energy Management of Plug-in Hybrid Electric Vehicles. *J. Power Sources* **2019**, *412*, 480–495. [[CrossRef](#)]
3. Lei, Z.; Sun, D.; Liu, Y.; Qin, D. Analysis and Coordinated Control of Mode Transition and Shifting for A Full Hybrid Electric Vehicle Based on Dual Clutch Transmissions. *Mech. Mach. Theory* **2017**, *114*, 125–140. [[CrossRef](#)]
4. Berkel, K.; Veldpaus, F.; Hofman, T.; Vroemen, B. Fast and Smooth Clutch Engagement Control for a Mechanical Hybrid Powertrain. *IEEE Trans. Control Syst. Technol.* **2014**, *22*, 1241–1254. [[CrossRef](#)]
5. Yang, C.; Song, J.; Li, L.; Li, S. Economical Vehicle Launching and Accelerating Control for Plug-in Hybrid Electric Bus with Single-shaft Parallel Hybrid Powertrain. *Mech. Syst. Signal Process.* **2016**, *76–77*, 649–664. [[CrossRef](#)]
6. Yang, C.; Jiao, X.; Li, L.; Zhang, Y. Robust Coordinated Control for Hybrid Electric Bus with Single-Shaft Parallel Hybrid Powertrain. *IET Control Theory Appl.* **2015**, *9*, 270–282. [[CrossRef](#)]
7. Jauch, C.; Tamilarasan, S.; Bovee, K.; Güvenc, L. Modeling for Drivability and Drivability improving Control of HEV. *Control Eng. Pract.* **2018**, *70*, 50–62. [[CrossRef](#)]
8. Zhao, Z.; Lei, D.; Chen, J.; Li, H. Optimal Control of Mode Transition for Four-Wheel-Drive Hybrid Electric Vehicle with Dry Dual-Clutch Transmission. *Mech. Syst. Signal Process.* **2018**, *105*, 68–89. [[CrossRef](#)]
9. Smith, A.; Bucknor, N.; Yang, H.; He, Y. Controls Development for Clutch-Assisted Engine Starts in A Parallel Hybrid Electric Vehicle. *SAE Tech. Pap.* **2011**. [[CrossRef](#)]
10. Xu, X.; Liang, Y.; Jordan, M.; Tenberge, P. Optimized Control of Engine Start Assisted by The Disconnect Clutch in A P2 Hybrid Automatic Transmission. *Mech. Syst. Signal Process.* **2019**, *124*, 313–329. [[CrossRef](#)]
11. Yang, C.; Jiao, X.; Li, L.; Zhang, Y. A Robust H_∞ Control-Based Hierarchical Mode Transition Control System for Plug-in Hybrid Electric Vehicle. *Mech. Syst. Signal Process.* **2018**, *99*, 326–344. [[CrossRef](#)]
12. Wang, X.; Li, L.; Yang, C. Hierarchical Control of Dry Clutch for Engine-Start Process in A Parallel Hybrid Electric Vehicle. *IEEE Trans. Transp. Electrification* **2016**, *2*, 231–243. [[CrossRef](#)]
13. Pisaturo, M.; Cirrincione, M.; Senatore, A. Multiple Constrained MPC Design for Automotive Dry Clutch Engagement. *IEEE/ASME Trans. Mechatron.* **2015**, *20*, 469–480. [[CrossRef](#)]
14. Li, L.; Wang, X.; Qi, X.; Li, X. Automatic Clutch Control Based on Estimation of Resistance Torque for AMT. *IEEE/ASME Trans. Mechatron.* **2015**, *21*, 1–13. [[CrossRef](#)]
15. Li, L.; Wang, X.; Hu, X.; Chen, Z. A Modified Predictive Functional Control with Sliding Mode Observer for Automated Dry Clutch Control of Vehicle. *J. Dyn. Syst. Meas. Control* **2016**, *138*. [[CrossRef](#)]
16. Gao, B.; Xiang, Y.; Chen, H.; Liang, Q. Optimal Trajectory Planning of Motor Torque and Clutch Slip Speed for Gear Shift of a Two-Speed Electric Vehicle. *J. Dyn. Syst. Meas. Control* **2015**, *137*. [[CrossRef](#)]
17. Gao, B.; Chen, H.; Liu, Q.; Chu, H. Position Control of Electric Clutch Actuator Using a Triple-Step Nonlinear Method. *IEEE Trans. Ind. Electron.* **2014**, *61*, 6995–7003. [[CrossRef](#)]
18. Gao, B.; Li, X.; Zeng, X.; Chen, H. Nonlinear Control of Direct-drive Pump-controlled Clutch Actuator in Consideration of Pump Efficiency Map. *Control Eng. Pract.* **2019**, *91*, 1–11. [[CrossRef](#)]
19. Gao, B.; Chen, H.; Sanada, K.; Hu, Y. Design of Clutch-Slip Controller for Automatic Transmission Using Backstepping. *IEEE/ASME Trans. Mechatron.* **2011**, *16*, 498–508. [[CrossRef](#)]
20. Park, J.; Choi, S.; Oh, J.; Eo, J. Adaptive torque tracking control during slip engagement of a dry clutch in vehicle powertrain. *Mech. Mach. Theory* **2019**, *134*, 249–266. [[CrossRef](#)]
21. Gatta, A.; Iannelli, L.; Pisaturo, M.; Senatore, A. A survey on modeling and engagement control for automotive dry clutch. *Mechatronics* **2018**, *55*, 63–75. [[CrossRef](#)]

22. Biswas, A.; Das, S.; Abraham, A.; Dasgupta, S. Design of fractional-order PID controllers with an improved differential evolution. *Eng. Appl. Artif. Intell.* **2008**, *11*, 1–8.
23. Monje, C.A.; Vinagre, B.A.; Feliu, V.; Chen, Y. Tuning and auto-tuning of fractional order controllers for industry applications. *Control Eng. Pract.* **2008**, *16*, 798–812.
24. He, L.; Shen, T.; Yu, L.; Feng, N. A Mode-Predictive-Control-Based Torque Demand Control Approach for Parallel Hybrid Powertrains. *IEEE Trans. Veh. Technol.* **2013**, *62*, 1041–1052. [[CrossRef](#)]
25. Li, Y.; Ang, K.; Chong, C. PID Control system analysis and design. *IEEE Control Syst. Mag.* **2006**, *26*, 32–41.
26. Igor, P. Fractional-Order Systems and $PI^\lambda D^\mu$ -Controllers. *IEEE Trans. Autom. Control* **1999**, *44*, 208–214.
27. Ranganayakulu, R.; Uday, G.; Seshagiri, A. A comparative study of fractional order $PI^\lambda/PI^\lambda D^\mu$ tuning rules for stable first order plus time delay processes. *Resour. Eff. Technol.* **2016**, *2*, 136–152. [[CrossRef](#)]
28. Zafer, B.; Oguzhan, K. Comparison of PID and FOPID controllers tuned by PSO and ABC algorithms for unstable and integrating systems with time delay. *Optim. Control Appl. Methods* **2018**, *39*, 1431–1450.



© 2019 by the authors. Licensee MDPI, Basel, Switzerland. This article is an open access article distributed under the terms and conditions of the Creative Commons Attribution (CC BY) license (<http://creativecommons.org/licenses/by/4.0/>).